

Optimal first-principles evaluation of electrostatic potentials: applications to interfacial band alignment and charged defect energies

Ravishankar Sundararaman^{1,2,*} and Yuan Ping^{1,3,†}

¹*These authors contributed equally.*

²*Department of Materials Science and Engineering,
Rensselaer Polytechnic Institute, Troy, NY 12180*

³*Department of Chemistry and Biochemistry,
University of California, Santa Cruz, CA 95064*

First-principles calculations of band alignment and charged defect formation energies require comparing electrostatic potential of different atomic configurations, which is made challenging by the strong oscillation of this potential at the atomic scale. We introduce a method to suppress these strong oscillations by eliminating the deep wells in the potential at each atom. We demonstrate that this method considerably improves the system-size convergence of a wide range of first-principles predictions that depend on alignment of electrostatic potentials, including band offsets at solid-liquid interfaces, and formation energies of charged vacancies in solids and at solid surfaces in vacuum. Finally, we use this method in conjunction with continuum solvation theories to investigate energetics of charged vacancies at solid-liquid interfaces. We find that for the example of an NaCl (001) surface in water, solvation reduces the formation energy of charged vacancies by 0.5 eV: calculation of this important effect was previously impractical due to the computational cost of molecular-dynamics methods.

First-principles calculations based on Kohn-Sham density functional theory (DFT) are used for calculating an ever-increasing range of material properties to provide atomic-scale insight into structures, interactions and dynamics. A particularly relevant class of material properties of recent interest involve the energetics of charged defects in bulk and surfaces, and electron transfer at solid-solid and solid-liquid interfaces. For example, the energy required to transfer an electron across a solid-liquid interface, which depends on the band alignment at this interface, critically determines the efficiency of photoelectrochemical cells for energy conversion.¹⁻³ The formation energies and charge transition levels of defects in bulk, surfaces and interfaces are extremely important for a host of applications including solar energy conversion,⁴ quantum computing,⁵ and light-emitting diodes.⁶ In this paper, we focus on a quantity that underlies the computation of both band alignment and charged defect energetics: the electrostatic potential profile in the material.^{7,8}

In plane-wave pseudopotential DFT calculations, the total electrostatic potential, including contributions due to both electrons and nuclei, is typically defined as

$$V(\mathbf{r}) = \underbrace{\int d\mathbf{r}' \frac{n(\mathbf{r}')}{|\mathbf{r} - \mathbf{r}'|}}_{V_H(\mathbf{r})} + \underbrace{\sum_i V_{\text{loc}}^{(i)}(|\mathbf{r} - \mathbf{r}_i|)}_{V_{\text{loc}}(\mathbf{r})}. \quad (1)$$

Above, $V_H(\mathbf{r})$ is the Hartree potential due to the valence electron density $n(\mathbf{r})$, and $V_{\text{loc}}(\mathbf{r})$ is the local part of the pseudopotential that includes the potential due to the nuclei and the core electrons, written as sum of spherical functions $V_{\text{loc}}^{(i)}$ centered at each nucleus located at \mathbf{r}_i .

This potential exhibits deep wells at each nucleus making averages of the potential highly oscillatory. For example, Fig. 1(a) shows the planarly-averaged electrostatic potential from a DFT calculation of an Ir(111) surface, which shows the characteristic deep wells at each (111) plane. Differences in the electrostatic potential between

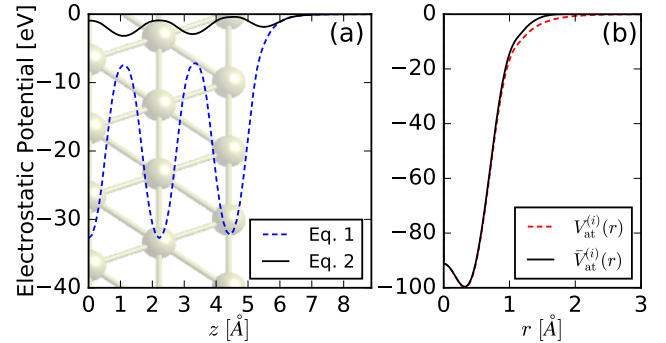


FIG. 1. (a) Comparison of the conventional (Eq. 1) and corrected (Eq. 2) planarly-averaged electrostatic potential for a 5-layer Ir(111) slab calculation. Note the drastic reduction of oscillations from the Hartree to eV scale. (b) Comparison of the original ($V_{\text{at}}^{(i)}(r)$) and pseudized ($\bar{V}_{\text{at}}^{(i)}(r)$) electrostatic potential of an Ir atom.

two calculations would cancel these deep wells provided the atoms in the two calculations can be aligned exactly, which is usually not possible when the ionic geometry is optimized. Consequently, all applications of DFT involving comparisons of electrostatic potential between systems with optimized ionic geometries require large enough unit cells that at least some of the atoms move negligibly and do not induce appreciable oscillations in the potential. This paper presents a method to minimize the magnitude of such oscillations, allowing more efficient and accurate smaller-unit-cell calculations for a number of such applications, including interfacial band alignment and charged defect formation energies.

Specifically, we eliminate the deep well in the potential at each nuclear position by subtracting the potentials of neutral atoms $\bar{V}_{\text{at}}^{(i)}$ centered at each nucleus, defining the

corrected electrostatic potential

$$\bar{V}(\mathbf{r}) = V_H(\mathbf{r}) + V_{\text{loc}}(\mathbf{r}) - \sum_i \bar{V}_{\text{at}}^{(i)}(|\mathbf{r} - \mathbf{r}_i|). \quad (2)$$

Effectively, this always defines the electrostatic potential of each calculation as a difference between two systems evaluated with atoms located at the same positions. (Formally, the second system is a collection of neutral atoms at the same positions that do not interact with each other.)

The electrostatic potential of neutral atoms $V_{\text{at}}^{(i)}$ is spherically symmetrical, exponentially decays away from the atom and can be easily and rapidly evaluated on a radial grid. It consists of the same two terms as Eq. 1: $V_{\text{loc}}^{(i)}(r)$ which is directly stored in atom pseudopotentials, and the Hartree potential which can be computed from the electron density by radial integration of the Poisson equation.

However, $V_{\text{at}}^{(i)}$ is not always localized to individual atoms, since the exponential decay of the atomic electron density can be slow. Consequently, subtracting $V_{\text{at}}^{(i)}$ would have the undesirable side effect of modifying the potential outside the atoms, where such a correction is not necessary. We therefore instead subtract a pseudized version, $\bar{V}_{\text{at}}^{(i)}$, of the neutral atom potential $V_{\text{at}}^{(i)}$, which is constructed to match $V_{\text{at}}^{(i)}$ in the core regions of the atom but smoothly approaches zero outside a cutoff radius R_i . Specifically we require that the corrected potential preserves the value, first and second derivatives at $r = 0$, and vanishes at R_i smoothly with zero first and second derivatives. The form of the corrected potential with the lowest order polynomial correction that achieves this is

$$\bar{V}_{\text{at}}^{(i)}(r) = \begin{cases} V_{\text{at}}^{(i)}(r) - \frac{r^3}{R_i^3} \left(a_3 + a_4 \frac{r}{R_i} + a_5 \frac{r^2}{R_i^2} \right), & r < R_i \\ 0, & r \geq R_i, \end{cases} \quad (3)$$

with the coefficients given by

$$\begin{pmatrix} a_3 \\ a_4 \\ a_5 \end{pmatrix} = \begin{pmatrix} 10 & -4 & 1/2 \\ -15 & 7 & -1 \\ 6 & -3 & 1/2 \end{pmatrix} \cdot \begin{pmatrix} V_{\text{at}}^{(i)}(R_i) \\ R_i \frac{dV_{\text{at}}^{(i)}}{dr} \Big|_{(R_i)} \\ R_i^2 \frac{d^2V_{\text{at}}^{(i)}}{dr^2} \Big|_{(R_i)} \end{pmatrix} \quad (4)$$

to satisfy the smoothness constraints at $r = R_i$.

The cutoff radius R_i is arbitrary, as long as it is small enough to avoid substantial overlap between neighbouring atoms, and it is large enough to encompass the core region so that it can eliminate the deep well in the potential. For definiteness, we follow the prescription for the vdW radius used in the DFT-D2 dispersion correction functional,⁹ and set $R_i = 1.1 \times$ the radius at which the electron density crosses $10^{-2} a_0^{-3}$. This also has the advantage of determining the radius from the electron density, and not requiring a tabulation of atomic radii for all elements.

Fig. 1(b) shows that the pseudized potential for an Iridium atom (using the GBRV ultrasoft pseudopotential¹⁰ for Ir), mostly follows the atom potential with only a

small correction that forces it to zero at finite radius. Using this pseudized atom potential in Eq. 2 then reduces the oscillations in the electrostatic potential by an order of magnitude relative to the original Eq. 1, as shown for the Ir(111) surface example in Fig. 1(a). The remainder of this paper shows that this reduction in the magnitude of the electrostatic potential oscillations considerably simplifies a number of DFT applications involving the potential, including band alignment and charged defect calculations.

Computational details: We implement the above method and perform all calculations here using the open-source plane-wave DFT software JDFTx.¹¹ We use the Perdew-Burke-Ernzerhoff generalized-gradient approximation¹² to the exchange-correlation functional, and ultrasoft pseudopotentials from the ‘GBRV’ set¹⁰ at the recommended kinetic energy cutoffs of $20 E_h$ for the wavefunctions and $100 E_h$ for the charge density. We use Monkhorst-Pack¹³ k -point grids for Brillouin zone sampling, with the number of k -points per dimension chosen to have a minimum supercell length of 20 \AA in each direction. For all surface calculations (slab geometry), we use truncated Coulomb potentials to eliminate interactions between periodic images of the slab across the vacuum (or liquid) region.¹⁴

Band offsets at solid-liquid interfaces: The electrostatic potential profile plays a central role in determining the energy level alignment across interfaces, which in turn affects the charge transport across interfaces. DFT calculations of the electrostatic potential are routinely used to calculate the energy level alignment across solid-solid interfaces, such as the Schottky barrier height in metal-semiconductor interfaces.^{15,16} Even in theories beyond DFT, such as many-body perturbation using the GW method,¹⁷ calculation of band alignment across an interface requires comparing electrostatic potentials between DFT calculations of the bulk materials and the interface.^{3,18-21}

Similar calculations for solid-liquid interfaces are considerably more challenging, requiring *ab initio* molecular dynamics to sample several thousands of configurations of the liquid.^{7,18} Solvation models, which directly replace the thermodynamically-averaged effect of the liquid with that of a continuum dielectric, can substantially simplify such calculations for solid-liquid interfaces by eliminating the need for sampling liquid configurations. Recent solvation models^{22,23} can accurately predict the band alignment at these interfaces in comparison to experimental measurements or *ab initio* molecular dynamics simulations, at a fraction of the effort.⁴

Our method for reducing electrostatic potential oscillations due to nuclei is applicable to all these cases of band alignment at solid/solid and solid/liquid interfaces; here we will first demonstrate the application for band edge shifts by using one layer of explicit water molecules with and without solvation models. Fig. 2(a) shows the shift of the electrostatic potential, ΔV , of a γ -monoclinic WO_3 (001) surface, modeled with an inversion-symmetric 4 layer slab, due to a layer of explicit water molecules alone (dashed lines) and additionally with an implicit sol-

vent model (solid lines). (For the purposes of this comparison, we consider the stoichiometric surface for simplicity; see Ref. 4 for a detailed analysis on the important role of surface oxygen vacancies at this surface.) These cases are shown when the potential is evaluated both using the original Eq. 1 scheme (thinner blue lines) and our corrected Eq. 2 scheme (thicker black lines). The strong binding of water molecules to the hydrophilic WO_3 surface perturbs the surface structure substantially, and this leads to strong oscillations in ΔV of magnitude over 2 eV extending into the inner layers in the original scheme. With exactly the same perturbed geometries, our correction scheme reduces the overall magnitude of the oscillations to within 0.1 eV, making the identification of the net band offsets (≈ 0.8 eV without and 1.0 eV with the solvation model) far clearer.

Similarly, Fig. 2(b) compares the ΔV induced by one layer of explicit water molecules added to the IrO_2 (110) surface, modeled with inversion-symmetric 5 and 7 layer slabs. As before, the correction scheme reduces oscillations from the ~ 1 eV scale to within the 0.1 eV scale, resulting in an essentially flat potential profile beyond the first unit cell of the surface. Note however that despite the strong oscillations in the original scheme, the potential shift at the center of the slab ($z = 0$) is not strongly affected by the correction scheme; this is because the central layer atoms do not change their z positions on account of the inversion symmetry of our slab. Indeed, Fig. 2(c) shows similar comparisons for a polar GaAs(111) surface which necessarily breaks inversion symmetry. In this case, the oscillations in the original scheme persist all the way through to the center of the slab, making identification of the net band offsets challenging, whereas our corrected scheme (Eq. 2) yields a flat ΔV profile beyond the first layer enabling unambiguous determination of the band offset (≈ 0.3 eV).

Formation energies of charged defects: Eliminating oscillations in the electrostatic potential improves system-size convergence, and hence reduces computational effort, more generally wherever alignment of this potential matters. We next demonstrate the efficacy of our method for a prominent example of increasing recent interest: the calculation of the formation energies and charge transition levels of charged defects such as vacancies.^{24–26} Briefly, the formation energy of a charged vacancy V_A^q of an atom A with net charge q , is given by

$$E_{\text{form}} = E_{\text{bulk}+V_A^q} - E_{\text{bulk}} + \mu_A - qE_{\text{Fermi}} + E_{\text{corr}}, \quad (5)$$

where the first two terms compare the energies of a supercell of the material with and without the vacancy, while the third and fourth terms account for the difference in numbers of atom A and electrons respectively with their corresponding chemical potentials. The fundamental challenge in calculating E_{form} is that $E_{\text{bulk}+V_A^q}$ converges very slowly with supercell size ($\propto L^{-1}$) due to the periodic interactions between the charge q .⁸ The final term E_{corr} estimates and compensates for these interactions by using a Gaussian charge model of the vacancy and calculating the difference between the self energy of that charge in isolation and in the finite supercell,

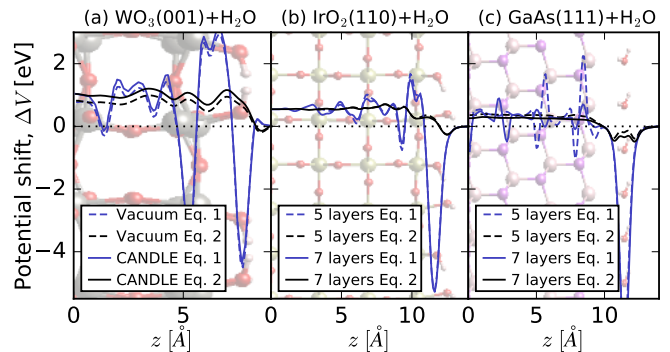


FIG. 2. Comparison between electrostatic potential shifts (ΔV) predicted using original (Eq. 1) and corrected (Eq. 2) schemes for the addition of an explicit monolayer of water molecules to (a) γ -monoclinic WO_3 (001) surface in vacuum and with the CANDLE solvation model,²³ and to (b) IrO_2 (110) and (c) GaAs (111) surfaces described using 5 and 7 layer slabs. Surface structures shown in the background are to scale with the x -axis. Substantial oscillations in ΔV in the original scheme are suppressed by our correction scheme (Eq. 2), making the potential converge to the bulk value in fewer layers.

in the background of the bulk dielectric constant of the material.²⁴ (The relevant dielectric constant is the low-frequency value ϵ_0 if the atoms are optimized, and the optical value ϵ_∞ if the atoms are fixed.) Additionally, it includes an ‘alignment’ contribution $-q\Delta V$ due to the difference in electrostatic potential of the model charge far from the defect compared to that calculated by DFT. This is necessary because of the indeterminacy of absolute potential in periodic boundary conditions. See Ref. 24 for further details.

Here, we apply this calculation scheme for the formation energy of $q = +1$ Cl vacancies in bulk NaCl, and examine the effect of our correction scheme on the alignment potential ΔV . Fig. 3(a) compares this potential, radially averaged from the center of the defect, as evaluated using Eqs. 1 and 2, both when the atom positions are fixed at their bulk values, and when they are optimized. When the atoms are fixed (dashed lines), the original and corrected schemes agree exactly beyond 2 Å, because the remaining atoms exactly overlay and the subtraction scheme has no effect. However, once the atoms are optimized, ΔV exhibits oscillations with magnitude ~ 0.5 eV 5 Å away and ~ 0.1 eV 10 Å away even after radial averaging in the original scheme, while our correction scheme yields a flat ΔV profile beyond $r = 5$ Å. Fig. 3(b) shows the corresponding predictions for the formation energies using the aforementioned method.²⁴ Note that optimizing the atom positions is extremely important here: it lowers the vacancy formation energy by greater than 1 eV. As expected from the ΔV comparison, the predicted formation energy for optimized atom positions using Eq. 1 for the potential, exhibits errors ~ 0.1 eV even for $1/L \sim 0.1\text{Å}^{-1}$, while the corrected scheme gives more accurate results with even smaller supercells of $1/L \sim 0.14\text{Å}^{-1}$. Furthermore, the results using Eq. 2 show a clear convergence for

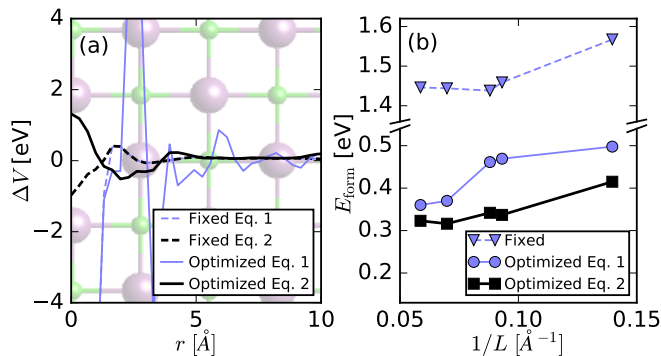


FIG. 3. (a) Alignment potential ΔV between DFT and Gaussian charge model for a $q = +1$ Cl vacancy in NaCl, averaged radially away from the vacancy, compared between Eq. 1 and 2, both for fixed and optimized atom positions. The crystal structure is shown in the background to scale with respect to the x -axis. (b) Corresponding convergence of the formation energy E_{form} of the $q = +1$ Cl vacancy with inverse supercell size, where $L = \Omega^{1/3}$ for supercell volume Ω . Reduced oscillations in ΔV using Eq. 2 enable accurate calculations of E_{form} with much smaller supercells (larger $1/L$).

the four larger supercells (smaller $1/L$ than $\sim 0.14 \text{ \AA}^{-1}$), while those of Eq. 1 do not. Overall, Eq. 2 enables results with better accuracy using supercells that are twice the $1/L$ i.e. that contain $1/8$ as many atoms, compared to what was previously possible with Eq. 1.

Charged defects at interfaces: Atoms at the surface of solid are usually less tightly bound than those in the bulk, and surfaces are often more prone to contain defects such as vacancies, and these can play an important role in determining interface potentials and band alignment.⁴ Calculating the formation energy of charged defects at surfaces conceptually follows the same procedure as the bulk case (Eq. 5), and encounters the same convergence issue due to periodic interactions of the charge, albeit now in two dimensions instead of all three. Fortunately, the correction scheme of Ref. 24 generalizes for defects at surfaces as well.²⁵ Intuitively, the only difference is that the self energy and potential of the model charge are calculated using a dielectric slab $\epsilon_0(z)$ (or $\epsilon_\infty(z)$ for fixed atoms) to mimic the remaining material, instead of a uniform dielectric covering all space for the bulk case. See Ref. 25 for a detailed exposition; we follow the same procedure except for two refinements. First, we improve the electrostatic potential using Eq. 2 as before, which we discuss below. Additionally, we develop a more robust and general method for evaluating the isolated self-energy of the Gaussian charge model with an arbitrary $\epsilon(z)$ background using a spectral expansion in cylindrical Bessel functions (see SI), instead of the image charge series method of Ref. 25.

In the surface case, the electrostatic potential plays an additional role in the determination of the dielectric slab model $\epsilon_0(z)$ (or $\epsilon_\infty(z)$). Specifically, we apply a uniform normal electric field E_0 to the DFT calculation of the slab, measure the change in the total electrostatic potential $\Delta V(z)$, and from that calculate the dielectric function

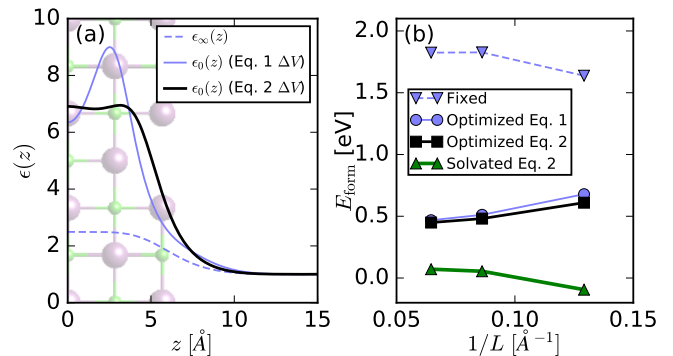


FIG. 4. (a) Dielectric profiles of 5-layer NaCl(100) slab calculated with fixed atom positions ($\epsilon_\infty(z)$) and optimized atom positions ($\epsilon_0(z)$), using either Eq. 1 or 2 for the electrostatic potential. The background shows the structure of this slab with a Cl vacancy (not included in dielectric calculation) to scale. (b) Convergence of formation energy of a $q = +1$ Cl vacancy at the surface of this slab with inverse supercell size, where $L = A^{1/2}$ for lateral supercell area A . Eq. 2 improves convergence, but less dramatically so than in the bulk case. Note that geometry optimization and solvation have large effects on vacancy formation energies.

using $\epsilon^{-1}(z) = (1/E_0)(-\partial\Delta V(z)/\partial z)$. This yields ϵ_0^{-1} or ϵ_∞^{-1} depending on whether the atoms are optimized or fixed. Fig. 4(a) shows the calculated dielectric profiles from potentials using Eqs. 1 and 2 for an inversion symmetric 5-layer NaCl(100) slab. The correction scheme has no effect by definition for $\epsilon_\infty(z)$ since the atoms are fixed. For $\epsilon_0(z)$, Eq. 1 produces oscillations with the lattice planes, despite the Gaussian smoothing, while Eq. 2 produces a smooth transition from 1 outside the slab to the bulk value inside it.

Fig. 4(b) shows the corresponding formation for $q = +1$ Cl vacancies. Once again, geometry optimization reduces the formation energy by a large amount (≈ 1.3 eV). However, in this case, the effect of the smoother electrostatic potential using Eq. 2 produces a less drastic improvement in the convergence with supercell size. The primary reason is that the convergence with lateral supercell size is already reasonable with Eq. 1, because in this case ΔV between DFT and the model charge can be aligned accurately in the vacuum region (outside the slab) which is not affected by the large oscillations due to atom displacements. Also note that unlike previous studies,²⁵ we do not need to worry about convergence with the length of the normal direction because we use truncated Coulomb potentials to exactly eliminate periodic interactions in that direction for all calculations (neutral and charged).¹⁴

Finally, our methods for solvation,²³ electrostatic potential evaluation and charged defect correction for arbitrary $\epsilon(z)$ models (see SI) make it possible now to straightforwardly predict formation energy of charged defects at solid-liquid interfaces. Intuitively, this only requires using the solvation model in both the energy calculations in Eq. 5, and including the solvent response contributions to the Gaussian charge model calculations. Fig.4(b) shows that our method continues to yield excel-

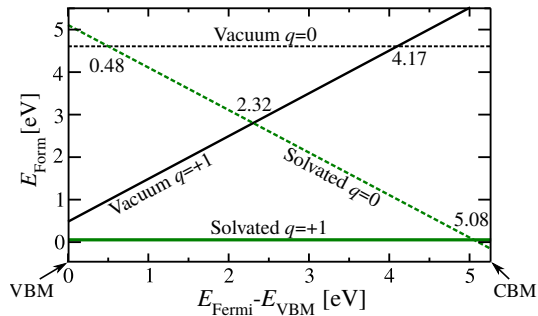


FIG. 5. Formation energies of neutral ($q = 0$) and charged ($q = +1$) Cl vacancies at an NaCl(001) surface in vacuum and solution, as a function of the Fermi level. Charged vacancies are more stable for most Fermi level positions in both cases, and vacancy formation is more favorable in solution overall.

lent supercell size convergence for the predicted formation energies of $q = +1$ Cl vacancies at an NaCl(001) surface in water. Note that the formation energies are strongly stabilized by about 0.5 eV relative to the vacuum surface.

An important qualitative difference also arises due to the choice of reference chemical potential of Cl, μ_{Cl} , in Eq. 5. In vacuum, the natural choice is set by molecular/gaseous Cl_2 , while in water, the natural choice is Cl^{-1}

ions in solution. Fig. 5 shows the variation of formation energies of neutral and charged Cl vacancies at NaCl(001) surfaces in vacuum and water with the Fermi level (or electron chemical potential). Note that the charged vacancy in water and neutral vacancy have zero slope; this is because without exchanging electrons, a Cl^{-} ion can leave the surface into solution, while a Cl atom can go to Cl_2 gas in vacuum. In both cases, the charged vacancy is more stable for most values of E_{Fermi} in the band gap, and the overall formation energies of vacancies are much smaller in solution than in vacuum.

In summary, we show that a simple correction scheme of subtracting pseudized atom potentials suppresses oscillations in DFT electrostatic potentials by over an order of magnitude. This makes it possible to efficiently and accurately predict band alignments at interfaces, and energetics of charged defects in solids, at surfaces and even at solid-liquid interfaces, with much smaller slab and supercell sizes. The substantial stabilization of charged defects at solid-liquid interfaces underscores the importance of evaluating charged defective surfaces in solution. While this was previously formidable due to the difficulty of dealing with electrostatic potential alignment in expensive molecular dynamics simulations, the combination of our correction scheme and continuum solvation theories make such calculations now practical compared with expensive molecular dynamics simulations.

* sundar@rpi.edu

† yuanping@ucsc.edu

- ¹ M. G. Walter, E. L. Warren, J. R. McKone, S. W. Boettcher, Q. Mi, E. A. Santori, and N. S. Lewis, *Chemical Reviews* **110**, 6446 (2010), pMID: 21062097.
- ² S. Chen and L.-W. Wang, *Chemistry of Materials* **24**, 3659 (2012).
- ³ Y. Ping, W. A. Goddard, and G. A. Galli, *Journal of the American Chemical Society* **137**, 5264 (2015).
- ⁴ Y. Ping, R. Sundararaman, and W. A. Goddard III, *Phys. Chem. Chem. Phys.* **17**, 30499 (2015).
- ⁵ A. Alkauskas, B. B. Buckley, D. D. Awschalom, and C. G. V. de Walle, *New J. Phys.* **16**, 073026 (2014).
- ⁶ A. Alkauskas, Q. Yan, and C. G. Van de Walle, *Phys. Rev. B* **90**, 075202 (2014).
- ⁷ T. Pham, Y. Ping, and G. Galli, *Nature Materials* **in press** (2016).
- ⁸ C. Freysoldt, B. Grabowski, T. Hickel, J. Neugebauer, G. Kresse, A. Janotti, and C. G. Van de Walle, *Rev. Mod. Phys.* **86**, 253 (2014).
- ⁹ S. Grimme, *J. Comput. Chem* **27**, 1787 (2006).
- ¹⁰ K. F. Garrity, J. W. Bennett, K. Rabe, and D. Vanderbilt, *Comput. Mater. Sci.* **81**, 446 (2014).
- ¹¹ R. Sundararaman, D. Gunceler, K. Letchworth-Weaver, K. A. Schwarz, and T. A. Arias, "JDFTx," <http://jdftx.sourceforge.net> (2012).
- ¹² J. P. Perdew, K. Burke, and M. Ernzerhof, *Phys. Rev. Lett.* **77**, 3865 (1996).

- ¹³ H. J. Monkhorst and J. D. Pack, *Phys. Rev. B* **13**, 5188 (1976).
- ¹⁴ R. Sundararaman and T. Arias, *Phys. Rev. B* **87**, 165122 (2013).
- ¹⁵ A. Baldereschi, S. Baroni, and R. Resta, *Phys. Rev. Lett.* **61**, 734 (1988).
- ¹⁶ M. Peressi, N. Binggeli, and A. Baldereschi, *Journal of Physics D: Applied Physics* **31**, 1273 (1998).
- ¹⁷ M. Govoni and G. Galli, *Journal of Chemical Theory and Computation* **11**, 2680 (2015).
- ¹⁸ T. A. Pham, D. Lee, E. Schwegler, and G. Galli, *Journal of the American Chemical Society* **136**, 17071 (2014), pMID: 25402590.
- ¹⁹ Y. Ping and G. Galli, *The Journal of Physical Chemistry C* **118**, 6019 (2014).
- ²⁰ Y. Ping, D. Rocca, and G. Galli, *Chem. Soc. Rev.* **42**, 2437 (2013).
- ²¹ Y. Hinuma, A. Grüneis, G. Kresse, and F. Oba, *Phys. Rev. B* **90**, 155405 (2014).
- ²² R. Sundararaman, K. A. Schwarz, K. Letchworth-Weaver, and T. A. Arias, *J. Chem. Phys.* **142**, 054102 (2015).
- ²³ R. Sundararaman and W. A. Goddard, *J. Chem. Phys.* **142**, 064107 (2015).
- ²⁴ C. Freysoldt, J. Neugebauer, and C. G. Van de Walle, *Phys. Rev. Lett.* **102**, 016402 (2009).
- ²⁵ H.-P. Komsa and A. Pasquarello, *Phys. Rev. Lett.* **110**, 095505 (2013).
- ²⁶ Y. Kumagai and F. Oba, *Phys. Rev. B* **89**, 195205 (2014).